Title: Differential tissue stiffness of body column facilitates locomotion of *Hydra* on solid substrates

Authors: Suyash Naik[1,2], Manu Unni[1], Devanshu Sinha[2], Shatruhan Singh Rajput[2], P. Chandramouli Reddy[1], Apratim Chatterji[2], Shivprasad Patil[2,*] and Sanjeev Galande[1,*]

Affiliations:

[1]Department of Biology, Indian Institute of Science Education and Research, Pune 411008, India
[2]Department of Physics, Indian Institute of Science Education and Research, Pune 411008, India

[*]To whom correspondence should be addressed.

Contact Information:
Sanjeev Galande
Centre of Excellence in Epigenetics, Department of Biology
Indian Institute of Science Education and Research
Dr. Homi Bhabha Road, Pune 411008, India
Tel: 91-20-25908060, Fax: 91-20-20251566
email: sanjeev@iiserpune.ac.in

And

Shivprasad Patil
Nanomechanics Laboratory, Department of Physics
Indian Institute of Science Education and Research
Dr. Homi Bhabha Road, Pune 411008, India
Tel: 91 20 25908034, Fax 91 20 20251566
email: s.patil@iiserpune.ac.in

Keywords: Biophysics, Locomotion, Extracellular matrix and *Hydra*

Abstract

The bell-shaped members of Cnidaria typically move around by swimming whereas the *Hydra* polyp can perform locomotion on solid substrates in aquatic environment. To address the biomechanics of locomotion on rigid substrates, we studied the 'somersaulting' locomotion in *Hydra*. We applied atomic force microscopy on the whole animal to measure the local mechanical properties of body column and identified the existence of differential Young's modulus between the shoulder region versus rest of the body column at 3:1 ratio. We show that this movement depends primarily on graded variations in tissue stiffness of the body column and is explained by computational models that accurately recapitulate the mechanics involved in this process. We demonstrate that perturbation of the observed stiffness gradient in hydra body column by modulating the extracellular matrix (ECM) polymerization impairs the 'somersault' movement. These results provide mechanistic basis for the evolutionary significance of differential ECM properties and tissue stiffness.

Main Text

Locomotion enables organisms to move from one place to another. The need to move around evolved very early in life forms, which accorded several advantages to the organisms. Locomotion offers exploration opportunities for food source, water source, mates, niche and more importantly, escaping predators. Morphological diversities and tissue type innovations facilitated in the evolution of various means of locomotion in different organisms. The organisms that use specialized appendages and body oscillations to propel themselves are often known to share common biomechanical principles (Biewener, 1990, Gray, 1933, Alexander, 2003). While unicellular organisms use dedicated organelles such as cilia, flagella or pseudopodia, the multicellular organisms exhibit a complex system of coordination among specific cell types to achieve locomotion (Bray, 2000). Basal metazoans evolved two types of locomotion- Fluid-dependent and substrate- dependent. Sponges are mostly sessile but some of them are known to move extremely slowly on the substrate it is attached to, using lamellipodia-dependent migration of motile cells at the base (Bond and Harris, 1988). Placozoans, on the other hand, can move about both in water and substrates using cilia of the cells (Ueda et al., 1999). Ctenophora are capable of moving exclusively in liquid using the comb plates (Ctenes), which are assisted by the beating of underlying cilia (Figure 1*A*) (Matsumoto, 1991). Organisms from these phyla, although capable of multicellular locomotion, do not possess specialized tissues as is the case with complex eumetazoans. Cnidarians, on the other hand, have acquired the ability to perform coordinated locomotion both in water and solid substrates and are the earliest phylum to evolve differentiated neuronal/muscular tissues and extracellular matrix (ECM) properties (Bode, 1996, Bode et al., 1990, Dupre and Yuste, 2017).

Cnidarians typically have two different types of body structures viz. the medusa and the polyp forms (Galliot, 2000). The medusal organisms such as Jellyfish mediate their movement with the help of thrust or pull of fluids using the umbrella, and hence are dependent on the mechanics of fluids (Gemmell et al., 2015, Anderson and DeMont, 2000). The direction of movement can be controlled by directing the fluid flow with the help of muscles (Anderson and DeMont, 2000). *Hydra* is a cnidarian polyp lacking the medusal stage in its life cycle. It has a very slender yet extremely flexible body column having equally flexible tentacles at the oral end. The flexibility of *Hydra* is primarily due to its unique ECM composition (Deutzmann et al., 2000). *Hydra* exhibits interestingly complex modes of locomotion capable of exploiting fluid and substrate for movement. *Hydra* polyps can simply float by generating small air bubbles at the basal disk (Figure 1*B*) (Mackie, 1974). Once afloat, these polyps move according to the water current and lose the bubble when it reaches a favourable location. The

more complex modes of locomotion utilize the neuro-muscular system present in *Hydra*. The muscular cells in the two germ layers are oriented orthogonally with respect to each other, which help in controlling both the length as well as the radial width of the organism (Aufschnaiter et al., 2017, Haynes et al., 1968). These muscular cells are controlled by different neural circuits to achieve a range of coordinated behavioural activities (Dupre and Yuste, 2017, Han et al., 2018, Davis et al., 1968). This ability of *Hydra* to contract and relax co-ordinately helps *Hydra* to perform a range of movements such as swaying, looping and somersaulting (Trembley, 1744). Looping is the more commonly seen form of locomotion where the *Hydra* extends, attaches to the substrate with tentacles and drags its base close to the hypostome. Then tentacles detach with its base firmly attached to the new position on the substratum (Figure 1*C*).

In the current study we have focused on the somersault, which involves co-ordinated movements with initial steps similar to looping but in entirety more complicated than looping. It includes adhering to the substrate with the tentacles for traction. The body is then moved around the head in a semi-circular arc with characteristic contractions (Figure 1*C*), which we observed and recapitulated using computational modelling. Even though the movement is not the same as walking, there are some interesting parallels that can be drawn such as the forces acting on these bodies and energy recycling to reduce muscular work. We tried to understand the substrate-based movements in *Hydra* somersault using a minimalistic elastic model and recapitulated part of the movement. We investigated the stiffness of the tissue along the body column to showed that the evolution of a differential in the stiffness could play a role in mediating these movements and discover that attaining ECM-dependent stiffness differential has been an ancient mechanism to accomplish specialized tissue function. In this study, we show that the tissue region with high stiffness assumes a musculoskeletal property to help *Hydra* pull off the somersaulting stunt.

Results

Hydra somersault is typically initiated by stretching the body column to almost double its length (stage 1, Figure 2*A*) and by attachment of the head to the substratum with the help of tentacles and hypostome (Trembley, 1744, Han et al., 2018). During this process, the region of body column just below the head referred to here as 'shoulder', is bent by almost 90º angle (stage 2). The basal disc at the bottom of the foot is then released, relaxing the stretched body column and accentuating the bend in the shoulder (stage 3). The bend straightens out (released) to achieve 'upside down' position of the body column perpendicular to the substratum (stage 4) (Figure 2*A*, Movie 1). The process is completed by bending the body column, followed by attachment of basal disc to a new position. Finally, the oral end pushes itself away with the help of tentacles and the body attains the upright position. The process after the stage 4 is achieved mostly through active force generation and hence is not focused on in this study.

Measurement of local variation in tissue stiffness

Multicellular organisms use spatially differentiated tissue types, such as exoskeleton in invertebrates or musculoskeletal systems as seen in vertebrates, to resist strain and sustain tractions during locomotion (Biewener, 1990, Dickinson et al., 2000). These specialized tissues exhibit differential stiffness properties, which help in locomotion. It was not known if *Hydra* possesses any tissue elasticity-dependent mechanisms to aid in its locomotion. We used atomic force microscopy (AFM) to produce a spatially resolved map of tissue elasticity for the first instance in *Hydra*. We measured the Young's modulus to record tissue stiffness at points ~100 µm apart (Figure 2- Figure supplement 2 *A*). We observed higher stiffness in the region below the base of tentacles, which extends up to 25 per cent of the length of the body column, referred to as the shoulder region. The shoulder region is nearly three-fold stiffer (Y =1480 ± 20 Pa) compared to the rest of the body (Y = 450 ± 6 Pa). For tentacles, the Young's modulus (Y) is 378 ± 11 Pa (Figure 2- Figure supplement 2). These measurements revealed a steep drop in stiffness at the junction of shoulder and the rest of the body column (Figure 2*B*, Figure 2 – figure supplement 2).

In *Hydra,* the novel sharp gradation in tissue elasticity leads to mechanically distinct behavior. The deformations under similar forces would be larger in the body column than the shoulder region and the restorative forces lower in the body column. This is interesting in context of the somersault, as initially the deformation is seen in the body column and the shoulder region is deformed in the later stages of the movement. The forces acting on *Hydra* to retard its movement in water are mainly viscous in nature. *Hydra*'s weight is mostly negated by the buoyant forces, leading to a reduced gravity

138 situation working against the uplift of the body column. We reasoned that to overcome the viscous and
139 reduced gravitational force on the body column in order to stand upside down, the energy stored in the
140 bent shoulder is utilized by the organism (Figure 2*D*). The observation that *Hydra*'s shoulder is three
141 times stiffer suggests that it allows the shoulder to store larger mechanical energy for a given bend.
142 The shoulder region can be viewed as a stiff spring with a high bending rigidity due to its higher
143 Young's modulus. Careful analysis of the mechanics of somersault reveals that after releasing from
144 basal end, the bend in the shoulder becomes pronounced. The force produced by a spring of a similar
145 stiffness as the shoulder undergoing physiological deformations would be capable of overcoming
146 gravitational forces and viscous forces. This hypothesis is supported by the observation that the *Hydra*
147 completely extends before release and the process post-release involves relaxation of the muscles back
148 to the original state (Figure 2*D*, Figure 2 – video 1).

149 To quantify the stored energy in the bend (E_{bend}) and its progression in time after release from
150 the basal end we recorded *Hydra* performing the somersault and measured the tissue strain in the
151 shoulder (Figure 3*A*, and Figure 2 – figure supplement 2). The energy stored was estimated by
152 calculating the strain as the curvature of the shoulder (R). The E_{bend} exhibited an initial increase with
153 time, suggesting a transfer of energy from the stretched body column to the bent shoulder (Figure 3*B*).
154 This suggests that after the release, the stretched body column could act as a motor generating energy
155 and storing a part of that energy in the stiff shoulder spring. (Figure 2*C*, Figure 2*D* and Figure 3*A*).
156

157 **Simulations predict importance of tissue stiffness variation in somersault**

158 To gain insights into the role of observed variation in tissue stiffness in facilitating efficient
159 transfer of mechanical energy to bend, we simulated the somersault. We modelled the tubular body
160 of *Hydra* by a suitable network of 50 rings of bead-springs, which are stacked together to form an
161 elastic cylinder of length L (Figure 4*A*). All springs have spring constant κ. The effective spring
162 constant of the cylinder is κ_{eff}. We observed that κ_{eff} varies linearly with κ. The experimentally
163 measured mass, length and Young's modulus of *Hydra* was used to convert simulation units of m, L
164 and κ_{eff} into physical units. To model the experimentally observed stiffness variation along the *Hydra*
165 body-column, we chose spring-constants κ of individual springs in the shoulder region to be α times
166 the remainder of the body column. In simulations, for the same amount of initial energy (30 nJ), α was
167 varied from 1 for uniform Y to relatively large value of 30 to investigate the importance of spatial
168 variation in tissue stiffness for the mechanics of somersault. Additionally, to truly represent the
169 physical environment we included viscous drag, the force of gravity and buoyancy, on each bead of
170 the model *Hydra* (Figure 4 – Figure supplement 1).

To model the role of elasticity in energy transfer from stretch to bend (Figure 3), we stretched the cylinder and fixed the two rings at the ends nearly horizontally with strain $\varepsilon = 0.8$ and 0.2. We then released the basal end, which has lower stiffness. Qualitatively, the somersault in real *Hydra* compares well with simulations for $\alpha = 3$ which is observed in AFM experiments. Interestingly, under uniform stiffness along the length of the cylinder ($\alpha = 1$), the model *Hydra* was unable to stand upside down after the release (Figure 4 – Figure supplement 2 and Movie 2-1), suggesting that the observed variation in tissue stiffness seems critical to complete the somersault. We experimentally measured the density of *Hydra* polyp and observed that it is 5.0 ±1.5 percent higher than the density of water.

We observe that before the release of the basal end, the potential energy (PE) stored in the shoulder for $\alpha= 3$ is lower than for $\alpha= 1$. This is due to the comparatively larger stretch in the shoulder for $\alpha= 1$. However, after release, roughly 50 percent more energy is transferred to the shoulder region for $\alpha= 3$ compared to $\alpha= 1$. The progression of energy stored in the shoulder after the end of horizontal movement of the basal end signifies the contraction (Figure 4*B*). The stored energy in the shoulder region at the end of contraction step is expended to overcome gravity and viscous drag. The energy threshold ($E_{threshold}$) required to stand upside down can be calculated (Figure 4*B*). For $\alpha= 1$, the stored energy in the shoulder is below this threshold, and for $\alpha= 3$ it is above it. This suggests that if *Hydra* body column were to harbor uniform stiffness, then it would not be able to stand up (Figure 4*B*). This result is robust with respect to different values of ε (Figure 4- Figure supplement 3).

To explain the physics behind the efficient energy transfer for $\alpha = 3$, we analyzed the simulation data. During contraction, it is observed that velocity difference between the shoulder and body column is larger for a model *Hydra* with non-uniform stiffness compared to uniform case ($\alpha=1$) (Figure4 – Figure supplement 4 and Figure supplement 5). This generates more force on the shoulder region while the body column contracts. We calculated time averaged longitudinal force on 14th ring, which is residing at the junction between the stiff shoulder and the labile body column (Figure 4*C*). Clearly, the force is higher for $\alpha= 3$. The bend in the shoulder, in turn, receives adequate potential energy for standing upside-down (Figure 4*B*). To find out the optimal variation of tissue stiffness for highest possible transfer we performed simulations for all values of α. Strikingly, the force does not increase monotonically with α but has a clear peak around $\alpha= 5$ which is close to 3. For large values of α (more than 20), the force is less than even the uniform case. This indicates that a specific variation in tissue stiffness characterized by α is optimal for energy transfer in *Hydra* somersault and large values of α do not ensure effective energy transfer. Collectively, the simulations indicated that the variation in tissue stiffness observed in AFM experiments is critical for somersault.

The simulations clearly show that the variation in tissue stiffness, characterized by α, facilitates efficient energy transfer from a stretch to a bend, which is used to overcome the downward force on the body column due to *Hydra*'s higher density compared to that of water. Since this energy is used for overcoming the hydrodynamic drag and the weight of body column due to the the density difference, the successful completion of somersault depends on two parameters specific to Hydra: Δρ and α. Since experimentally observed Young's modulus is over-estimated owing to the treatment with Glutaraldehyde, we generated phase diagrams Δρ versus α for different values of Young's modulus. We observed that for extremely labile bodies (Y < 10 Pa), the energy stored in the stretch and transferred to the bend is lower than the threshold and Hydra is unable to rise for all values of α. On the other hand, for extremely stiff bodies (Y > 10 kPa), the energy required to stretch to 80 percent strain is large and the transferred energy is always above the threshold such that *Hydra* is always able to rise for all values of α. These two extremes are far from the experimentally observed stiffness and its variation in real *Hydra* tissue. Figure 4D depicts the phase diagram of Δρ and α at the experimentally observed values of Y. Note that in order to keep the amount of energy and strain fixed when the model *Hydra* is stretched, for α < 3, Y for the body region is kept larger than 500 Pa. For α > 3, the Y for the body region is kept smaller than 500 Pa. For Y= 500 Pa throughout the body column, it is not able to rise and stands inverted if the tissue is 2.5 percent denser than water. The parameters Δρ and α for real *Hydra* lie inside the green oval shape (Figure 4D). The phase diagram is robust with respect to strain and different initial energies stored in the stretch. It clearly indicates that a model *Hydra* with larger α, signifying a better energy transfer, can lift itself even if its heavy, which is described by a larger Δρ. It is also interesting that the critical behaviour for lifting the body column is seen in the phase plot of Δρ and α only for the range of tissue stiffness seen in real *Hydra*.

The experimentally measured stiffness of *Hydra* tissue is likely to be an overestimate due to treatment of Glutaraldehyde. It has also been reported that such treatment does not largely affect tissue stiffness. It is difficult to quantify such effect in case of *Hydra*, but the observed increase in Young's modulus due to such treatment on rat-tail tendons quantified using AFM is nearly 50 percent (Hensen et al, 2009). We have performed simulation runs to monitor the effect of such overestimates on critical nature of standing upside down. Figure 4 - Figure supplement 6 A shows a phase diagram in which, Y for both shoulder and body column is halved compared to the experimentally observed values in our AFM experiments. The variation characterized by α is seen to be more critical than that depicted in Fig. 4D. *Hydra* with uniform stiffness is unable to lift its body column, even if it is 1 percent above the density of water.

236 **Modulation of ECM polymerization perturbs the tissue stiffness variation, impairing the**
237 **somersault**

238 To identify the source of tissue stiffness and its differential, we hypothesized two possibilities,
239 i.e. variation in the cell types or differences in ECM composition. A recent report suggested that there
240 is no difference in cellular stiffness in *Hydra* cells and hence we ruled out the possibility of cellular
241 contribution (Carter et al., 2016). Stiffness variation due to ECM composition could be tested by
242 selectively disrupting physical properties of mesoglea without disrupting the chemical composition
243 avoiding the possibility of disturbing Integrin-ECM interactions. *Hydra* mesoglea (ECM) is a
244 trilaminar porous structure which divides the two germ layers throughout the polyp and is in a
245 perpetually stretched state (Sarras Jr, 2012). Therefore, any lesion to the mesoglea leads to retraction
246 of the mesoglea from the site of injury (Sarras Jr, 2012, Shimizu et al., 2002). The outermost layer of
247 ECM is similar to the basement membranes consisting of cell-interacting ECM proteins such as
248 collagen type IV and laminins (Sarras Jr, 2012). On the other hand, the layer being sandwiched by the
249 basement membrane called the interstitial matrix, is mainly made up of fibrillar collagens such as
250 collagen type I, II, III, IV and hence can provide mechanical support to the polyp (Sarras Jr, 2012).

251 Based on these properties we have devised physical and chemical perturbations to mitigate the
252 stiffness of ECM. In the physical method, we exploited the retractile property of ECM to locally disrupt
253 stiffness which would sever the hypothetical 'spring' (Figure 5*A*). Whereas the chemical method uses
254 Dipyridyl (DP), a lysyl oxidase inhibitor, to inhibit polymerization of the newly secreted fibrillar
255 collagen into fibrils in ECM and therefore globally affecting the physical property of newly
256 synthesized ECM as it replaces old without changing its composition (Figure 5B) (Shimizu et al., 2002,
257 Sarras et al., 1991, Siegel et al., 1970).

258 On two different sets of *Hydra* polyps, we partially lesioned the shoulder region and the middle
259 of the body column severing the ECM. Then we recorded the somersaults performed after 6 hours after
260 lesion (Figure 5A, Figure 5- Figure supplement 1B, Movie 3-1). This time was chosen as it is sufficient
261 to heal the wound but not enough for regaining the stiffness around the lesion since ECM is not fully
262 regenerated (Sarras et al., 1991, Shimizu et al., 2002). Strikingly, the ability to perform somersaults is
263 virtually lost when the lesion is in the shoulder region whereas it remains unaffected when it is in the
264 body column (Figure 5A). The polyps with a lesion in the shoulder were able to regain the ability to
265 somersault after 36 hours, duration long enough for complete ECM regeneration. Thus, elimination of
266 the stiffness locally within the shoulder region results in an inability to perform the somersaults,
267 underscoring the importance of the stiffness gradient. The AFM measurements revealed that the polyps
268 treated with DP for 72 hours exhibit uniform stiffness across the entire body column (Figure 5 – Figure

supplement 1A). This suggests that *Hydra* has presumably utilized differential crosslinking of fibrillar collagen to generate tissues with varying degree of elasticity. The ability to somersault was completely lost after 72 hours of DP treatment whereas the number of somersaults was reduced to half after 36 hours of treatment (Figure 5B and Movie 3-2). This confirms the correlation of the degree of unpolymerized fibrillar collagen in the ECM to the inability to somersault. These observations suggest that the ECM mediated stiffness gradient in the *Hydra* polyp is critical for somersaulting.

In the third experiment, the animals with a lesion in the shoulder region were treated with DP. This does not allow the regeneration of ECM in the nicked region. In this case, even after 36 hours of the nick, polyps were unable to regain the propensity to somersault (Figure 5*C* and Movie 3-3). Collectively, these findings provide compelling evidence that spatial variation in tissue stiffness is critical for the somersault, corroborating the results of the simulations.

Discussion

We report the first ever use of atomic force microscopy for measuring the tissue stiffness of *Hydra* along the whole body-column. We have obtained more definitive results than the earlier reports of tissue stiffness in *Hydra* (Carter et al., 2016). Here, we demonstrated that *Hydra* possesses a local 3:1 variation in tissue stiffness between the shoulder region to the rest of the body column.

To understand the significance of such a sharp gradient in the body column we investigated the seemingly strenuous process of somersaulting (Biewener, 1990). The simulations revealed that the discontinuous gradient in stiffness is necessary for energy transfer to stand upside down. In congruence with simulations, the *Hydra* polyps lacking the stiffness gradient were unable to stand upside down during somersault. The differential speeds of shoulder and rest of the body during retraction leads to a soft collision between the two regions, which results in an efficient transfer of energy from the body column to the stiff region (shoulder). Further, the differential stiffness of the body column enables the animal to strike an optimal balance between the mechanical energy stored in the stretching and the bending processes. While stretched, most of the energy is stored in the labile body column due to the extension. The collision allows for the energy produced in the extension step to be concentrated into potential energy in the bend of the shoulder region. Comparing the somersault to walking on land, the arrangement of the shoulder and the body column acts similar to the movements of legs. The tentacles allow for stability by providing lateral forces similar to insect legs (Dickinson et al., 2000). The shoulder region acts as a spring storing energy from the stretched body column and repurposing it to lift vertically. While somersaulting allows the polyp to move around in the immediate environment in intermediate distances, looping allows the polyps to cover smaller distances. For larger distance

locomotion, floating with air bubble would be more favorable. Whereas, the labile part of the body column can extend with relative ease allowing the *Hydra* to probe its immediate surroundings without moving to a new position and expending too much energy. We also observed in our experiments that the polyps showed a higher propensity to perform looping, somersaulting or stretching when we detached them and dropped them back in culture bowl. This behavior can be explained by the need for *Hydra* to probe the immediate surrounding to gauge the nature of new site when it settles in natural conditions. Such probing might be important in obtaining different sets of information by the polyp including water flow differential in the surrounding, better substrate attachment sites, prey abundance etc.

The arrangement of the shoulder and the body column can be compared to that of tendons and muscles in vertebrates. The spring mechanism in the shoulder region is similar to mechanisms proposed for motion during terrestrial walking (Markowitz and Herr, 2016, Taylor and Heglund, 1982). Energy recycling through tendons and other elastic elements is an established mechanism in describing locomotion in vertebrates such as humans (Cavagna et al., 1977). Tendons consist of thick bundles of collagen fibers secreted by tenocytes. Incidentally, tenocytes can change the ECM composition of tendons in response to changes in mechanical loading and hence the elasticity (Kjaer, 2004). Based on our study, mechanisms modulating elastic properties of tissues to facilitate locomotion seems to have evolved early in the animal phyla and hence seems to be an ancient function of the ECM. It points to the possibility that shear stresses faced during tentacle movement as well as the structural peculiarities of the organism may have played a role in evolving the stiffness differential (Carter et al., 2016, Shostak et al., 1965, Haynes et al., 1968). The torsional forces for moving a flexible rod-like structure as tentacle in water could be of the range of nanonewton/micronewton and deformations in the hypostome would be of the order of nanonewton. Such scales of repetitive deformations could have led to the evolution of mechanosensory feedback mechanisms required for regulating the ECM stiffness. One of the easiest ways to achieve the same is by modulating the crosslinking of fibrillar collagens in the ECM, an example of which we have illustrated here. A similar mechanism might have further evolved in more complex higher organisms during the development of the musculoskeletal system.

Our study provides significance to the observed changes in cellular and molecular properties at the shoulder region. The cellular movement shows a marked difference between the shoulder region and the body column (Holstein et al., 1991). All the cells in a polyp are known to be pushed towards the termini of the body and sloughed off. The ECM associated with these cells is also reported to move along with these cells and degraded at the tentacle tip or the basal disk (Aufschnaiter et al., 2011).

Strangely, the aforesaid behavior changes at the shoulder region with a reduction in the cell-ECM velocities. This could be due to differential interactions of cells with the ECM components in the shoulder region versus the rest of the body column, as has been proposed earlier (Shostak et al., 1965). ECM is degraded within the shoulder region than being pushed to the tentacles indicating that ECM in this region is maintained in a different manner as opposed to other regions. Further, BrdU staining indicates a cessation of proliferative capacity of the stem cell as they cross the boundary towards the shoulder region and into the hypostome and tentacles (Reddy et al., 2015). In *Hydra,* the tentacles and the hypostome region possess a wide range of differentiated cells, which terminally differentiate as they move from the gastric region towards the hypostome and tentacles (Wood, 1979, Ewer and Fox, 1947). It would be interesting to study if, similar to human and mice cells, stiffness properties of the ECM determine the differentiation fate of these cells in *Hydra* (Engler et al., 2006, Park et al., 2011). Thus, tissue stiffness in *Hydra* is not only innately linked to the motility of the organism but also possibly other processes.

Collagen, as shown here, plays an important role in the tissue stiffness, possibly both through cell-ECM interactions and varying ECM composition (Shostak et al., 1965, Aufschnaiter et al., 2011, Zhang et al., 2007, Shimizu et al., 2008, Sarras Jr, 2012). The collagen fiber structure in the ECM can be dynamically regulated depending on the strain experienced locally (Haynes et al., 1968). Studies need to be performed to understand how collagen and other ECM molecules are regulated along the oral-aboral axis of *Hydra*. Our findings not only open a new avenue in invertebrate locomotion mechanics which could lead to interesting insights into the evolution of locomotion but also lay a foundation for furthering mechanobiology in the lower organisms using AFM. Additionally, the need of an optimal elasticity variation for greater energy efficiency in liquid environments could be a significant design principle for building artificial machines and advance the field of the untethered small-scale robots working in confined areas (Hu et al., 2018).

Methods and Materials

1. *Hydra* lines and culture

The polyps used were the Pune strain of *Hydra vulgaris* (Ind. Pune) and *Hydra vulgaris* (AEP) (Reddy et al., 2011, Martínez et al., 2010). *Hydra* polyps were cultured under standard conditions in glass bowls with *Hydra* medium containing KCl, NaCl, $MgSO_4.7H_20$, $CaCl_2.7H_2O$ and Tris-HCl using the protocol described previously (Lenhoff, 2013). Both lines were maintained at 19ºC and with a day night cycle of 12 hours. Polyps were fed using freshly collected Artemia hatched in house. The medium was changed every day after feeding.

2. Measurement of *Hydra* tissue stiffness using atomic force microscope (AFM)

2.1. Attaching bead to the AFM lever:

A tipless cantilever with a glass bead attached to its free end (stiffness ~ 0.2 N/m) was used for AFM measurements. The diameter of the glass bead is 20 µm (Figure 2 – Figure supplement 1). The attachment was accomplished using the micromanipulation available with the AFM. A small amount of UV curable glue (Dymax 431) was spread on the coverslip. Using the servo control of the AFM, the end of the tipless lever was lowered onto the glue. A drop of glue was picked up on the lever and lowered again on a bead. The lever was maintained under positive load and UV light was directed at the bead-lever assembly. After curing the lever was pulled back from the surface along with the bead. The elastic modulus of the glue is 570 MPa and it is not deformed while pushing on the tissue. Before performing force- distance measurements, the cantilever is calibrated using BSA coated glass surface by thermal tuning.

2.2. Measurement of tissue stiffness using AFM:

Hydra body is unstable for mechanical measurements if it is not strongly adhered to the glass surface. A thin layer of BSA was coated on the glass for strong adherence of the tissue. Young's modulus of various tissues typically ranges from 100 Pa to 1 MPa. The Young's modulus of glass is of the order of 10-100 GPa. The coating of BSA alters it to some extent. Figure 2 – Figure supplement 2 shows the cantilever deflections for glass, BSA coated glass and tissues from different parts along body column. Assuming the glass-glass contact to be infinitely stiff compared to the glass-tissue contact - a reasonable assumption since it is 10,000 times stiffer, the slope of the curve in the contact region for glass and BSA coated glass is nearly one implying no deformation. The slope of the curve on tissues is much less suggesting certain amount of deformation. We use glass-glass contact for calibration of deflection sensitivity and the subtraction of cantilever deflection from the push given by the piezo extension yields deformation in the tissue. The force is calculated by multiplying the

cantilever deflections by its stiffness. The force versus deformation curve is then fitted with Hertz model.

$$F = \frac{E}{1-v^2}[\frac{a^2+R_s^2}{2} ln \frac{R_s+a}{R_s-a} - aR_s]$$

$$\delta = \frac{a}{2} ln \frac{R_s+a}{R_s-a}$$

Where F is the measured by the cantilever possessing the bead, which is pressed against the tissue. R is the bead radius, delta is the deformation in the tissue, E is Young's modulus and v is Poisson ratio.

Hertz contact mechanics theory works for non-adhesive elastic contacts. It is important to establish that the pressing of bead over the tissue conforms to this requirement. Figure 2 –Figure supplement 1 B shows a typical force-deformation measurement while both extending and retracting the bead over the tissue. For small loads (< 1 nN) the extend and retract curves do not show hysteresis indicating that the contact is non-adhesive and elastic.

Before AFM measurements, *Hydra* were cultured and starved for a day to eliminate food material. They were relaxed with urethane (2% for 2 mins) and fixed immediately with glutaraldehyde (4%) for 30 mins. The coverslip (diameter: 22 µm) was coated with a layer of bovine serum albumin (BSA, 10 mg/ml), and this layer was allowed to dry. The *Hydra* was placed on this layer, and a small amount of BSA was added to keep it from drying. As the BSA dried, the connections formed between the *Hydra* and the surface by BSA were fixed using glutaraldehyde for 2 min and water was added.

3. Videography and analysis of somersault

We recorded the motion of *Hydra* as it does the somersault movements and measured the statistics of somersaults with modification of native stiffness along body column (Figure 5). We fabricated a glass tank of 10 x 8 x 4.5 cm dimensions and recorded the movement using a Nikon D-500 digital camera fitted with a 105 mm macro lens. The *Hydra* movement was recorded as they detached from the surface. For measurement of distances a precise scale was kept in the bath. The videos were recorded at 25 fps for 20 min at a stretch. We assayed the propensity of *Hydra* to somersault after dropping them with a pipette into the tank. For the ease of scoring, we have only scored the number of times polyps stand upside-down since it is the first and most important step for *Hydra* to somersault. The normalization of the events was done by calculating the average and standardizing the values by comparison to the control. The videos were analyzed with the light works software and Fiji. Circles were fit to the shoulder region of *Hydra* using Fiji software and the bend energy stored in the shoulder region was measured. The radii of circles measured at different times was used to calculate the bending energy using:

$$U = \frac{YIL}{2R^2}$$

$$I = \int r^2 dA = \frac{\pi(r_1^4 - r_2^4)}{4}$$

Where U is the bending energy, L is the length of the shoulder region in hydra (25% of body column), Y is the young's modulus of the shoulder region (stiffer spring), R is the radius of the circle fit using Fiji, I is the second area moment of inertia, r is the perpendicular distance of an elemental area dA along the axis of bending, r_1, r_2 are the outer and inner radii of the hydra body column respectively. The change in energy was seen from the point of detachment from the substrate to the final vertical native state of the *Hydra.*

4. Hydra simulations

4.1 Model-*Hydra*:

This cylinder now behaves like a network of springs having effective spring constant κ_{eff}. We show that the response to an axial deformation of the cylinder is equivalent to that of a spring of spring constant κ_{eff}, where κ_{eff} varies a maximum of 20% for small to large strains and increases linearly with increase of κ_{ind} (Figure 4 – Figure supplement 1*B* and *C*). Since the cylinder shows a resistance to stretching and bending under application of suitable external forces, the κ_{eff} can be taken to be a measure of the Young's modulus of the cylinder. To calculate κ_{eff}, we fix the position of the mass-points at one end, stretch the other end axially such that the strain of the cylinder is $\epsilon = (L - L_0)/L_0$ and measure the force F_{axial} acting on the ring of 10 mass-points at the other end due to the stretching of all the constituent springs. The quantity is defined to $k_{eff} = F_{axial}/(L - L_0)$ (Figure 4- Figure supplement 1 *A* and *B*). The linearity of κ_{ind} with implies that we can suitably choose κ_{eff} along the *Hydra*'s body column to mimic the variation in its elasticity.

4.2 Comparison of motion of model-*Hydra* and *Hydra:*

We schematically depict two stages of model-*Hydra* motion in Figure 4 - Figure supplement 2 *A*. We describe the external forces acting on the model *Hydra* during the simulations. The somersault motion of *Hydra* lies in a low Reynolds number R_e) regime. We integrate the Newton's equations of motion using a modified velocity verlet algorithm which incorporates Stoke's drag, Γ_i (Drag coefficient of ith mass point). The expression for the drag coefficient of a long thin cylinder along the axis perpendicular to its axial length is given by $\Gamma_\perp = 4\pi\eta L/ln(L/D)$ while $\Gamma_\parallel = 0.5\Gamma_\perp$, where $\Gamma_\parallel$ is the drag coefficient when cylinder moves parallel to axis. Since *Hydra* performs a combination of longitudinal (along the axis contraction) and transverse motion (upwards motion) and has the same order of magnitude, an average of $\Gamma_\parallel$ and $\Gamma_\perp$ has been used in the

simulations, i.e., $\Gamma = (\Gamma_\perp + \Gamma_\parallel)/2$. Thereby each mass point experiences a drag force with the drag coefficient $\Gamma_i = \Gamma/500$ (since there are 500-point masses in 50 rings linked by springs), such that the total drag force results from the drag coefficient of Γ.

In Figure 4 – Figure supplement 2 *B* the motion of a stretched *Hydra* (left panel) and a stretched cylindrical network of springs (right panel) with $\alpha = 3$, i.e. the stiffness variation as seen at the shoulder in *Hydra*. When the ring of unit-masses at the shoulder-end remains fixed on and the other end is released. The strain $\varepsilon = (L - L_0)/L_0$, is kept at $\varepsilon = 0.8$. Here, L is measured as the displacement of the center of the last ring at the basal end (which gets released) from the center of the first ring at the shoulder-end, whereas L_0 is the neutral or relaxed length of the system. After release, a series of snapshots show the relaxation to be very similar for the spring network and real *Hydra*: in the first stage the axis of the cylinder stays close to the horizontal surface as the cylinder contracts in length till nearly its equilibrium length L_0, but remains bent. In the second stage the model *Hydra* releases its bending energy as the object straightens as it moves through the background water/liquid by overcoming the viscous drag and gravitation. The bending energy stored in stiffer shoulder region thus appears to play a crucial role. To emulate the solid floor on which the real *Hydra* rests, we added a repulsive Lennard-Jones interaction at the plane below the cylinder, such that the Simulation *Hydra* does not cross the z=0 plane (shown by dotted horizontal line) plane in snapshots.

4.3 Units:

The experimentally observed values of the length of the Hydra body column is around 5 mm while its inner and outer radii are 0.05 mm and 0.1 mm respectively. In our simulation this is modeled as a hollow cylindrical tube of diameter of a = 1 simulation units (s.u) and length $L_0 = 30a$ (see Table 1).

Table 1

Dimension	**Simulation Units**	**SI Units**
Length [L]	a =1	0.17×10^{-3} m
Mass [M]	$m_i = 1$	2×10^{-10} kg
Time [T]	$\tau = 1$	0.91×10^{-3} s

The stretched elastic body of Hydra can be physically characterized by its Young's modulus Y, stored elastic energy E, length L, cross-sectional area A (found using its inner and outer radii) and its

mass M= $\sum m_i$, whereas viscous drag due to liquid surrounding *Hydra* can be characterized by the viscous drag coefficient Γ. These parameters can be combined to form a dimensionless parameter *D*.

$$D = \frac{\Gamma L^{3/2}}{E}\sqrt{\frac{YA}{M}}$$

Substituting $k_{eff}=k_{ind}$ = YA/L, which is essentially replacing the Young's modulus by the stiffness constant of an equivalent spring, gives us

$$D = \frac{\Gamma L^{2}}{E}\sqrt{\frac{k}{M}}$$

We can estimate these parameters in the following way:

a) <u>Elastic energy (E):</u>

We take the experimentally measured value of the Young's modulus around 1000 Pa, we assume the stress strain relationship linear, i.e. σ = Yε. Stored elastic energy per unit volume is given by the integral of the stress-strain curve. For the sake of simplicity, we take energy per unit volume, stored at a strain of ε = 1.

$$E/V = \int_0^1 \sigma d\epsilon \implies E = V\int_0^1 Y\epsilon d\epsilon = \frac{YV\epsilon^2}{2}|_0^1 = \frac{YV}{2}$$

Using the values of inner and outer radii for the Hydra as well as its length of 5 mm, we get the energy value of the elastic energy to be

$$E = \frac{YV}{2} = \frac{10^3 Pa \times \pi(1^2 - 0.05^2) \times 10^{-8} m^2 \times 5 \times 10^{-3}}{2} \approx 6 \times 10^{-8} J$$

b) <u>Stoke's friction coefficient for a Cylinder (Γ)</u>:

The drag force experienced by the Hydra body column is determined by its Stoke's coefficient. The diameter to length ratio D/L of Hydra is small fraction, suggesting that it can be approximated as a long thin cylindrical tube (Akhtar et al., 2011, Dhont, 1996). The drag coefficient under this

$$\Gamma^{\parallel} = \frac{2\pi\eta L}{ln(L/D)}, \Gamma^{\perp} = \frac{4\pi\eta L}{ln(L/D)}$$

approximation is divided into two parts one parallel to the cylinder axis (running along its length), which we call $\Gamma^{||}$, and the other perpendicular to the axis Γ. Ideally, $\Gamma^{||}$ acts during the initial contractile motion of the Hydra, whereas $\Gamma^{||}$ acts during the upward motion. The expressions for these coefficients are

Here, L and D are length and diameter of Hydra body, while η is the viscosity of water, which is the environment they exist in. It can be seen that $\Gamma^{||} = \Gamma^{\perp} 2$. Since both these values do not defer by an order of magnitude, we take their average value as the drag coefficient

$$\Gamma = \frac{\Gamma^{||} + \Gamma^{\perp}}{2} = \frac{3\pi\eta L}{ln(L/D)}$$

Putting the viscosity of water as 10^{-3} Pa, L = 5 x10^{-3} m and D = 10^{-4} m, we get Γ = 1.2 x 10^{-5} Ns/m

c) <u>Mass (M)</u>:

We can assume *Hydra*'s body to have a mass density close to that of water, and thus its mass can be estimated as *Hydra*'s volume multiplied by the density of water. This comes out to be about 10^{-7} kg.

d) <u>Stiffness Constant of equivalent spring (k_{eff}):</u>

We use the relation of *k* to calculate this as

$$k = \frac{YA}{L} = \frac{10^3 Pa \times \pi(r_{outer}^2 - r_{inner}^2)}{L} \approx 0.5 \times 10^{-2} N/m$$

Using these values, the theoretically estimated value of the dimensionless parameter D is calculated as

$$D = \frac{\Gamma L^2}{E}\sqrt{\frac{k}{M}} = \frac{(1.2 \times 10^{-5} Pa)(5 \times 10^{-3} m)^2}{6 \times 10^{-8} J}\sqrt{\frac{0.5 \times 10^{-2} N/m}{10^{-7} kg}} \approx 1.1$$

The simulation parameters are chosen such that this dimensionless quantity remains unchanged when calculated using the simulation units. A choice of a stiffness constant fixes the stored elastic energy of the system. Using the effective stiffness value of 20 s.u, the stored energy can be calculated as ½ k_{eff} Δxsim^2. The neutral length of the simulation Hydra being 30 s.u., upon being stretched to twice its length gives the value of Δx_{sim}= 30 s.u. Using these values along with the simulation mass as 500 s.u. (each bead being assigned a mass of 1unit, with 500 beads forming the cylinder), we get

$$D^{sim} = \frac{\Gamma_{sim} L_{sim}^2}{E_{sim}} \sqrt{\frac{k_{sim}^{eff}}{M_{sim}}} = 0.02\Gamma_{sim} = D = 1.1$$

Solving for Γ_{sim}, the value of the Stoke's coefficient for the cylinder in simulation units can be calculated to be Γ_{sim}= 55 s.u. Since our mass-spring system consists of 500 beads, each bead can be assigned a viscous Stoke's coefficient of Γ_{sim}/(no. of beads) = 55/500 s.u. = 0.11 s.u.

e) <u>Time:</u>

We can construct a unit of time using the drag coefficient, Γ, neutral length of the Hydra, L0 and the elastic energy stored upon strain of ε = 1 as

$$\tau = \frac{\Gamma L^2}{E}$$

Having fixed the Stoke's coefficient from the previous steps, we are now in a position to calculate a correspondence between the real time units and the simulation time units. Since all the parameters are known, we have

$$\tau_{sim} = \frac{\Gamma_{sim} L_{sim}^2}{E_{sim}} = \frac{55 \times 30^2}{9000} = 5.5 s.u.$$

This must be equal to the real time units

$$\tau = \frac{\Gamma L^2}{E} = \frac{1.2 \times 10^{-5} Ns/m \times (5 \times 10^{-3})^2 m}{6 \times 10^{-8} J} = 5 \times 10^{-3} s$$

Comparing these two yields

$$1s = \frac{5.5}{5 \times 10^{-3}} = 1.1 \times 10^3 s.u$$

We have explicitly shown (see next section) that keeping the quantity $\Gamma_{sim} L_{sim}^2/E_{sim}$ constant yields the same relaxation behavior of the model.

The height of the basal disc from the floor versus time plots for ε = 0.2 for three different values of Γ_{sim} such that the value $\Gamma_{sim} L_{sim}^2/E_{sim}$ remains constant (with corresponding changes in E_{sim}). We can see that the evolution in time is exactly the same, justifying its choice as the experimental time scale.

f) Estimation of $E_{Threshold}$:

We estimate the threshold energy required to overcome both viscous drag and gravitation by first performing a continuous integration of the drag force (per bead) along the path traced by each bead as the model-Hydra evolves in time from its configuration at the end of the contraction to its final configuration (inverted position). Since only the model-Hydras with $\alpha > 1$ are able to reach this final configuration, we perform this integration for $\alpha = 3$. The sum of all such integrals (over all 500 beads which constitute the cylinder) gives us the total drag energy dissipated from initial (after contraction) to final configuration. We must add to this the gravitational potential energy of the final configuration ($\sum mgh$), which is obtained by summing over the gravitational potential energies of each bead in their final configuration. $E_{Threshold}$ can then be formally written as:

$$E_{Threshold} = \sum_{i}^{500} \int_{t_c}^{t_{final}} \gamma v_i(t) ds_i(t) + \sum_{i}^{500} m_i g' h_i$$

Here g' is the effective the gravitational acceleration used for calculation. It is only a small fraction of the actual gravitational acceleration (g) to account for buoyancy resulting from density difference between Hydra tissue and water.

4.4 Model-*Hydra* simulation results:

To quantify our observations of Figure 4 – Figure supplement 2 and setting forces due to gravity and buoyancy =0, we plotted the displacement of the tip of the cylinder at the basal end (Xbasal) moving in the horizontal direction (in the x-direction) in Figure 4 – Figure supplement 3A. Similarly, the Zbasal, the displacement in the vertical direction (along z-axis) is shown in Figure 4 – Figure supplement 3 B. The total potential energy and the total kinetic energy of the springs as a function of time is shown in Figure 4- Figure supplement 3 C and D, respectively. The horizontal plane is z = 0. At time t = 0, center of the basal ring is fixed at 1 mm and the ring at the end of the shoulder is fixed at x = 10.0 mm. This implies strain of 0.8 for Hydra with L0 = 5 mm. One observes that the displacement along X (Figure 4 – Figure supplement 3A) increases rapidly in the first step without much change in the displacement along Z (Figure 4 - Figure supplement 3 B). This initial displacement is identified as the contractile motion of the *Hydra*. Thus, the potential energy till this point of time is stored in the stretch, which then gets transferred to bend in the shoulder. In the second stage, wherein the basal disc moves vertically, this bending energy is dissipated to overcome the viscous drag as the

Hydra stands inverted. Therefore, we observe a decrease in the total potential energy as a function of time in Figure 4 – Figure supplement 3C.

We note that without factoring in gravity and buoyancy, the model *Hydra* is always able to stand inverted. We now investigate the relaxations of position of basal disc and energy (Figure 5*A-D*) for a cylinder with α = 1(uniform stiffness) and α =3 (non-uniform as seen in the experiments). To have a meaningful comparison with the case when α = 3, we choose the spring constant κ_U, such that a cylinder with uniform stiffness has the same energy as non- uniform stiffness for ε = 0.8. We see in Figure 4 – Figure supplement 3 *A* and *B* that the spring-network with the α = 3 stands inverted faster than α = 1, despite both having same initial energy.

Furthermore, it is observed in the simulations that the vertical motion (Figure 4- Figure supplement 3 *B*) of the model *Hydra* has the same functional form as a single spherical mass moving under the influence of stokes drag with initial conditions $z(0) = 0$ and $dz/dt|_{t=0} = v_0$, and satisfying the differential equation $\frac{d^2z(t)}{dt^2} + \frac{\Gamma}{m}\frac{dz(t)}{dt} = 0$. Upon solving the differential equation, we obtain $z(t) = a(1 - e^{-t/\tau}) + b$. We take z(t) with free parameters a, b and τ as the fit function, shown by the dashed lines in Figure 4 - Figure supplement 3 *B*. The parameter τ is defined as the relaxation time and is used to determine the relaxation time for different values of α.

It has been discussed in the Units section and as shown in Figure 4 Figure supplement 3E that τ for a given value of α is uniquely determined by the ratio of stokes drag coefficient Γ and the initial stored potential energy of the stretched model *Hydra*. Three different initial stored energy values were chosen by changing the stiffness of individual springs between mass-points, for a fixed strain of $\epsilon = 0.8$. Corresponding drag coefficients Γ were chosen such that the ratios drag and energy remains the same, i.e., $\Gamma_1/E_1 = \Gamma_2/E_2 = \Gamma_3/E_3$. It can be seen in the figure that all three curves overlap, suggesting that the relaxation is completely determined by the ratio of initial stored elastic energy and the drag coefficient. This also suggests that the unit of time can be constructed out of these parameters, as $\tau_R = \Gamma L_0^2/E$, where L_0 is the neutral length of the *Hydra*.

4.5: Phase diagram for criticality of standing inverted:

The downward force on *Hydra* body column while trying to stand inverted is due to density difference (Δρ) in *Hydra* tissue and water. The efficiency of energy transfer to work against this is large for greater stiffness variation (larger α). We have performed simulation runs for different parameters and we plot a phase diagram of Δρ and α to find out criticality for standing inverted. The simulations correctly predict the ability of lifting the body column against viscous forces and gravity. A *Hydra* with no variation in its tissue stiffness is always able to rise if the stiffness values are above 10 kPa.

Similarly, the for stiffness values less than 10 Pa, variation in tissue stiffness does not make the *Hydra* stand inverted for any value of α. For intermediate values of Y, which are closer to experimentally observed using AFM, the variation in tissue stiffness becomes critical for the somersault movement. Figure 4 Figure supplement 6 A shows the phase diagram for stiffness values which are halved compared to Figure 4D. Figure 4 Figure supplement 6 B shows phase diagram for strain of 0.2. The diagrams show criticality of standing upside down with respect to Δρ and α.

5. Density of Hydra and buoyancy:

In our simulations we performed the calculations for two situations. We initially assumed that the Hydra has nearly the same density as water. In this scenario, the buoyancy and gravity balance each other and the force due to gravity is set to zero. This was useful to define physical units of various quantities and to have access to energy stored in different parts of *Hydra* as it performs somersault. We could simulate hydra having uniform stiffness as well as the one having stiffness variations seen in experiments and characterized by α. The density of real *Hydra* tissues is larger density than that of water. This produces a downward force, which opposes the vertical motion after the contractile step. Interestingly, the model *Hydra* is always able to stand upside down if we ignore this downward force completely. We varied the magnitude of this force by tuning gravitational force on the *Hydra* to factor in buoyancy due *Hydra*'s additional density compared to water. We realized that six percent density difference is enough so that the model *Hydra* with uniform stiffness is not able to rise up against gravitational force. It is possible to measure density of *Hydra* by a following experiment. We remove tentacles and drop a Hydra in water column in a vertical tube (height 2 m, diameter 5 cm). It attains terminal velocity and is measured to be 0.003 m/s. It moves downwards horizontally without rotating or tumbling (Movie 2-2). After balancing forces acting on a cylindrical body moving with a terminal velocity in a fluid, we get

$$\rho = \rho_0 + \frac{4\pi\eta L/ln(L/D).v}{Vg}$$

Where ρ is density of hydra, ρ_0 and η are density and viscosity of water respectively. L is length of Hydra body column, D is diameter of the body column and V is volume of Hydra, g is acceleration due to gravity. We measured hydra length and diameter of at five different locations across the body column and measured it on 10 different animals. The errors in measurement of L and D largely determine errors in estimating the density of hydra from the measurements. The density of hydra tissue is 1050 ±15 kg/m^3. This is 5±1.5 % above the density of water.

654 **6. ECM disruption**

655 Hydra ECM has been shown to be dynamically regulated and important in regeneration as well. It
656 has been seen before that an amputation leads to a retraction of the ECM near the wound. This
657 retraction is about 100 μm below the cut edge and the ECM re-secretion takes about 24 hours to
658 complete (Sarras et al., 1991). We used this property of the ECM to physically perturb it upon nicking
659 (partial cut/amputation) of the organism. The nicking of *Hydra* is performed using the sharp bevel
660 edge of a 31-guage syringe needle and carefully controlled under a 10X dissection microscope.
661 Adequate care is taken such that the nick always is halfway through the body (incision upto half of the
662 diameter of the polyp at the shoulder region) and perpendicular to the long body axis, such that the
663 severed part does not move away. It is assured that the head attaches in the same place and the wound
664 is healed to carry out the videography of the somersaulting locomotion. Such amputation would lead
665 to a loss of ECM in a small region around the partial amputation. To assess the effect of loss of ECM
666 in a particular region on the stiffness of the organism we performed AFM on head partially cut polyps.
667 To assess the effect of localized ECM perturbation on ability of hydra to somersault, the polyps were
668 video graphed for somersault 6 hrs post amputation. These polyps were scored for "Events per hydra".
669 The scoring was performed by counting total number of occurrences the polyps performed upside-
670 down movement from the time they were dropped in the container floor for the first 5 mins. These
671 movements are labelled as "events" and these events were then divided by total number of polyps in
672 the container to get the value of "events per hydra" (Figure 5).

673 2,2'-Dipyridyl (DP) is an inhibitor of lysyl oxidase (Siegel et al., 1970). Lysyl oxidase is an enzyme
674 which cross-links two adjacent fibrillar collagens to make bundles. Inhibition of lysyl oxidase prevents
675 the components of the ECM from polymerizing. This has been shown before in being effective in
676 inhibition of *Hydra* ECM [6]. The concentration of 100 μM was shown to be useful in other strains of
677 *Hydra*. To test the validity of this result and to study the behavior of *Hydra* under this drug
678 concentration from 50 μM to 200 μM DP in *Hydra* medium were tested and no physiological effects
679 were detected until 175 μM. For the partial amputation along with DP treatment experiments (Figure
680 5), the organisms were pre-treated with DP for 12 hours followed by nicking and further treatment
681 with DP for 24 hours. *Hydra* ECM is continuously cycling along the body column and replenished.
682 For the DP experiments (Figure 5), DP was added to *Hydra* medium at 100 μM and the medium was
683 changed every 24 hours. AFM measurements were performed on *Hydra* treated for 72 hours to assess
684 the effect of chemical ECM disruption on the stiffness.

685

686

687 **Key resources table**

Reagent type (species) or resource	Designation	Source or reference	Identifiers	Additional information
gene ()	NA	NA		
strain, strain background (Hydra vulgaris)	Hydra vulgaris Ind Pune	Reddy, P.C. et. al.		
strain, strain background (Hydra vulgaris)	Hydra vulgaris AEP	Martinez, D. et. al.		
genetic reagent ()	NA	NA		
cell line ()	NA	NA		
transfected construct ()	NA	NA		
biological sample ()	NA	NA		
antibody	NA	NA		
recombinant DNA reagent	NA	NA		
sequence-based reagent	NA	NA		
peptide, recombinant protein	NA	NA		
chemical compound, drug	Tipless Cr-Au coated 38 series	Mikromasch	Cat. No: HQ:CSC38	/tipless/Cr-Au
chemical compound, drug	Dymax Ultra Light-Weld 431	Dymax	Lot no.: 527919	
chemical compound, drug	Micro glass beads	Corpuscular labs	Cat No: 149107-40	
chemical compound, drug	2,2' - Dipyridyl	Sigma-Aldrich	Cat. No: D216305	
software, algorithm	Jpk data processing software	Jpk instruments	Ver 5.1.8	
software, algorithm	R	https://www.r-project.org/	ver 3.4.4	
software, algorithm	Rstudio	https://www.rstudio.com/	version 3.4.4	
software, algorithm	Fiji	https://fiji.sc/	version 2.0.0+D8	

software, algorithm	Inkscape	https://inkscape.org	ve 3.4.4	
software, algorithm	blender	https://www.blender.org/about/	Version 2.79b	
software, algorithm	Liightworks	https://www.lwks.com/	Version 14.0	
software, algorithm	xmgrace	http://plasmagate.weizmann.ac.il/Grace/	Version 5.1.22	
software, algorithm	VMD	https://wwws.ks.uiuc.edu/Research/vmd	Version 1.9.3	

Acknowledgments

We would like to thank Drs Sudhakaran Prabhakaran and Sanjay Sane for useful comments on the manuscript. We thank Yashodeep Matange and Kanchan Sharma for help with animations and Dr Arpita Roychoudhury, Jitesh Seth and Adarsh Kumar for assistance with experiments. This work was supported by a grant from the Centre of Excellence in Epigenetics program (BT/01/COE/09/07) of the Department of Biotechnology, Government of India (SG), and computational grant (BT/PR/16542/BID/7/654/2016) from the Department of Biotechnology (AC); intramural funds from IISER Pune (DS, SR, SG, SP and AC); Department of Biotechnology postdoctoral fellowship (PCR), the Wellcome Trust-Department of Biotechnology India Alliance for Intermediate Fellowship (500172/Z/09/Z) (SP) and Early Career Fellowship (PCR); Department of Science and Technology, Govt. of India SERB grant No EMR/2015/000018 (AC); fellowships from the University Grants Commission (UGC) (MU), Kishore Vaigyanik Protsahan Yojana (KVPY) (SN), and Infosys foundation for international travel support (MU).

Footnotes

To whom correspondence should be addressed. E-mail: sanjeev@iiserpune.ac.in and s.patil@iiserpune.ac.in

The authors declare no conflicts of interest.

References

AKHTAR, R., SHERRATT, M. J., CRUICKSHANK, J. K. & DERBY, B. 2011. Characterizing the elastic properties of tissues. Materials Today, 14, 96-105.

ALEXANDER, R. M. 2003. Principles of animal locomotion, Princeton University Press.

ANDERSON, E. J. & DEMONT, M. E. 2000. The mechanics of locomotion in the squid Loligo pealei: locomotory function and unsteady hydrodynamics of the jet and intramantle pressure. Journal of Experimental Biology, 203, 2851-2863.

AUFSCHNAITER, R., WEDLICH-SÖLDNER, R., ZHANG, X. & HOBMAYER, B. 2017. Apical and basal epitheliomuscular F-actin dynamics during Hydra bud evagination. Biology open, 6, 1137-1148.

AUFSCHNAITER, R., ZAMIR, E. A., LITTLE, C. D., ÖZBEK, S., MÜNDER, S., DAVID, C. N., LI, L., SARRAS, M. P. & ZHANG, X. 2011. In vivo imaging of basement membrane movement: ECM patterning shapes Hydra polyps. J Cell Sci, 124, 4027-4038.

BIEWENER, A. A. 1990. Biomechanics of mammalian terrestrial locomotion. Science, 250, 1097-1103.

BODE, H. R. 1996. The interstitial cell lineage of hydra: a stem cell system that arose early in evolution. Journal of cell science, 109, 1155-1164.

BODE, H. R., GEE, L. W. & CHOW, M. A. 1990. Neuron differentiation in hydra involves dividing intermediates. Developmental biology, 139, 231-243.

BOND, C. & HARRIS, A. K. 1988. Locomotion of sponges and its physical mechanism. Journal of Experimental Zoology Part A: Ecological Genetics and Physiology, 246, 271-284.

BRAY, D. 2000. Cell movements: from molecules to motility, Garland Science.

CARTER, J. A., HYLAND, C., STEELE, R. E. & COLLINS, E.-M. S. 2016. Dynamics of mouth opening in Hydra. Biophysical journal, 110, 1191-1201.

CAVAGNA, G. A., HEGLUND, N. C. & TAYLOR, C. R. 1977. Mechanical work in terrestrial locomotion: two basic mechanisms for minimizing energy expenditure. American Journal of Physiology-Regulatory, Integrative and Comparative Physiology, 233, R243-R261.

DAVIS, L. E., BURNETT, A. L., HAYNES, J. F., OSBORNE, D. G. & SPEAR, M. L. 1968. Histological and ultrastructural study of the muscular and nervous systems in Hydra. II. Nervous system. Journal of Experimental Zoology Part A: Ecological Genetics and Physiology, 167, 295-331.

DEUTZMANN, R., FOWLER, S., ZHANG, X., BOONE, K., DEXTER, S., BOOT-HANDFORD, R., RACHEL, R. & SARRAS, M. 2000. Molecular, biochemical and functional analysis of a novel and developmentally important fibrillar collagen (Hcol-I) in hydra. Development, 127, 4669-4680.

DHONT, J. K. 1996. An introduction to dynamics of colloids, Elsevier.

DICKINSON, M. H., FARLEY, C. T., FULL, R. J., KOEHL, M. A. R., KRAM, R. & LEHMAN, S. 2000. How Animals Move: An Integrative View. Science, 288, 100-106.

DUPRE, C. & YUSTE, R. 2017. Non-overlapping neural networks in Hydra vulgaris. Current Biology, 27, 1085-1097.

ENGLER, A. J., SEN, S., SWEENEY, H. L. & DISCHER, D. E. 2006. Matrix elasticity directs stem cell lineage specification. Cell, 126, 677-689.

EWER, R. & FOX, H. M. On the Functions and Mode of Action of the Nematocysts of Hydra. Proceedings of the Zoological Society of London, 1947. Wiley Online Library, 365-376.

GALLIOT, B. 2000. Conserved and divergent genes in apex and axis development of cnidarians. Current opinion in genetics & development, 10, 629-637.

GEMMELL, B. J., COLIN, S. P., COSTELLO, J. H. & DABIRI, J. O. 2015. Suction-based propulsion as a basis for efficient animal swimming. Nature communications, 6, 8790.

758 GRAY, J. 1933. Studies in animal locomotion: I. The movement of fish with special reference to the
759 eel. Journal of experimental biology, 10, 88-104.
760 HAN, S., TARALOVA, E., DUPRE, C. & YUSTE, R. 2018. Comprehensive machine learning
761 analysis of Hydra behavior reveals a stable basal behavioral repertoire. elife, 7, e32605.
762 HAYNES, J. F., BURNETT, A. L. & DAVIS, L. E. 1968. Histological and ultrastructural study of
763 the muscular and nervous systems in Hydra. I. The muscular system and the mesoglea.
764 Journal of Experimental Zoology Part A: Ecological Genetics and Physiology, 167, 283-293.
765 HOLSTEIN, T. W., HOBMAYER, E. & DAVID, C. N. 1991. Pattern of epithelial cell cycling in
766 hydra. Developmental Biology, 148, 602-611.
767 HENSEN, P., HASSENKAM, T., SVENSSON, R. B., AAGAARD, P., TRAPPE, T.,
768 HARALDSSON, B. T., KJAER, M., and MAGNUSSON, P. 2009. Glutaraldehyde cross-
769 linking of tendon—mechanical effects at the level of the tendon fascicle and fibril.
770 Connective tissue research, 50, 211-222.
771 HU, W., LUM, G. Z., MASTRANGELI, M. & SITTI, M. 2018. Small-scale soft-bodied robot with
772 multimodal locomotion. Nature, 554, 81.
773 KJAER, M. 2004. Role of extracellular matrix in adaptation of tendon and skeletal muscle to
774 mechanical loading. Physiological reviews, 84, 649-698.
775 LENHOFF, H. 2013. Hydra: research methods, Springer Science & Business Media.
776 MACKIE, G. 1974. Locomotion, flotation, and dispersal. Coelenterate biology, 313-357.
777 MARKOWITZ, J. & HERR, H. 2016. Human leg model predicts muscle forces, states, and
778 energetics during walking. PLoS computational biology, 12, e1004912.
779 MARTÍNEZ, D., INIGUEZ, A., PERCELL, K., WILLNER, J., SIGNOROVITCH, J. &
780 CAMPBELL, R. 2010. Phylogeny and biogeography of Hydra (Cnidaria: Hydridae) using
781 mitochondrial and nuclear DNA sequences. Molecular Phylogenetics and Evolution, 57, 403-
782 410.
783 MATSUMOTO, G. Swimming movements of ctenophores, and the mechanics of propulsion by
784 ctene rows. Hydrobiologia, 1991. Springer, 319-325.
785 PARK, J. S., CHU, J. S., TSOU, A. D., DIOP, R., TANG, Z., WANG, A. & LI, S. 2011. The effect
786 of matrix stiffness on the differentiation of mesenchymal stem cells in response to TGF-β.
787 Biomaterials, 32, 3921-3930.
788 REDDY, P. C., BARVE, A. & GHASKADBI, S. 2011. Description and phylogenetic
789 characterization of common hydra from India. Current Science, 101, 736-738.
790 REDDY, P. C., UNNI, M. K., GUNGI, A., AGARWAL, P. & GALANDE, S. 2015. Evolution of
791 Hox-like genes in Cnidaria: Study of Hydra Hox repertoire reveals tailor-made Hox-code for
792 Cnidarians. Mechanisms of development, 138, 87-96.
793 SARRAS JR, M. P. 2012. Components, structure, biogenesis and function of the Hydra extracellular
794 matrix in regeneration, pattern formation and cell differentiation. International Journal of
795 Developmental Biology, 56, 567-576.
796 SARRAS, M. P., MEADOR, D. & ZHANG, X. 1991. Extracellular matrix (Mesoglea) of Hydra
797 vulgaris: II. Influence of collagen and proteoglycan components on head regeneration.
798 Developmental biology, 148, 495-500.
799 SHIMIZU, H., AUFSCHNAITER, R., LI, L., SARRAS JR, M. P., BORZA, D.-B.,
800 ABRAHAMSON, D. R., SADO, Y. & ZHANG, X. 2008. The extracellular matrix of hydra
801 is a porous sheet and contains type IV collagen. Zoology, 111, 410-418.
802 SHIMIZU, H., ZHANG, X., ZHANG, J., LEONTOVICH, A., FEI, K., YAN, L. & SARRAS, M. P.
803 2002. Epithelial morphogenesis in hydra requires de novo expression of extracellular matrix
804 components and matrix metalloproteinases. Development, 129, 1521-1532.
805 SHOSTAK, S., PATEL, N. & BURNETT, A. 1965. The role of mesoglea in mass cell movement in
806 Hydra. Developmental biology, 12, 434-450.

SIEGEL, R. C., PINNELL, S. R. & MARTIN, G. R. 1970. Cross-linking of collagen and elastin. Properties of lysyl oxidase. Biochemistry, 9**,** 4486-4492.

TAYLOR, C. R. & HEGLUND, N. C. 1982. Energetics and mechanics of terrestrial locomotion. Annual Review of Physiology, 44**,** 97-107.

TREMBLEY, A. 1744. Mémoires pour servir à l'histoire d'un genre de polypes d'eau douce, à bras en forme de cornes. Par A. Trembley, chez Jean & Herman Verbeek.

UEDA, T., KOYA, S. & MARUYAMA, Y. K. 1999. Dynamic patterns in the locomotion and feeding behaviors by the placozoan Trichoplax adhaerence. Biosystems, 54**,** 65-70.

WOOD, R. L. 1979. The fine structure of the hypostome and mouth of hydra. Cell and tissue research, 199**,** 319-338.

ZHANG, X., BOOT-HANDFORD, R. P., HUXLEY-JONES, J., FORSE, L. N., MOULD, A. P., ROBERTSON, D. L., LI, L., ATHIYAL, M. & SARRAS, M. P. 2007. The collagens of hydra provide insight into the evolution of metazoan extracellular matrices. Journal of Biological Chemistry.

823 **Figure Legends:**
824
825 **Figure 1. Locomotion in marine invertebrates.**
826 **A.** Ctenophora move around using comb cell or ctenae. They move efficiently with the help of ciliated
827 cells arranged in the form of combs and are one of the earliest and largest multicellular organisms
828 to do so. Photograph taken by R. Griswold/NOAA, distributed under a CC-BY 2.0 license.
829 **B.** Floating mode of locomotion in *Hydra* using an air bubble trapped at the aboral end of Hydra. It
830 allows for a passive mode of locomotion to flow along with currents in a natural habitat.
831 **C.** Looping mode of locomotion in *Hydra* involves bending the body column and pulling the body
832 column along.
833
834 **Figure 2. Somersault of *Hydra* and local variation in tissue stiffness.**
835 **A.** Schematic representation of the somersault movement of *Hydra* depicting various stages from
836 initiation to the upside-down position.
837 **B.** The plot of variation in Young's modulus (Y) along the body column measured using AFM
838 equipped with a bead-attached cantilever. The distance from tentacle base is plotted in units of
839 percentage of total body length. The ribbon indicates the standard deviation of mean over 25
840 measurements at each point and replicated over three organisms. The cartoon of *Hydra* shows
841 schematic representation of variations in Y in different regions of *Hydra*. The first quarter of the
842 body column is three times stiffer than the rest.
843 **C.** The forces and their direction of action are shown with the arrow denoting the direction. F_B
844 represents the force of buoyancy faced by the organism in water acting against the F_G gravitational
845 force faced by the organism. The drag force experienced is denoted by F_D acting against the
846 direction of motion. F_{Bend} is the representation of the force acting on the head region to store energy
847 in the bend. The changes in forces as the *Hydra* goes from Stage 1/Stage 2 (dotted outline) to Stage
848 4 (dotted outline)/Stage 5 can be seen.
849 **D.** The stiffer shoulder region is depicted as a hypothetical spring. The *Hydra* and the deformations
850 in this spring are shown as *Hydra* somersaults to reach the upside-down position. See also Figure
851 2 supplement 1 and Figure 2 supplement 2 A & B.
852
853
854
855
856
857
858

Figure 3. The energy transfer occurring in the stiff shoulder during somersaulting.

A. A schematic to illustrate the calculation of energy stored in the bent shoulder using $U = \frac{YIL}{2R^2}$. The shoulder region of the *Hydra* is fitted to a circle to measure the radius of curvature (R) of the bend. The length (L) is 25% of the total length (the stiff region) and Y is the Young's modulus as measured by AFM measurements. I is the second moment of inertia.

B. The energy in bend (E_{bend}) versus time, after the release (t= 0), increases to a peak. The energy exponentially decays as the bend straightens to bring the body to an upside-down position. The continuous line represents a fit to a single exponent (τ~ 0.4 s).

Figure 4. Simulations unravel significance of the stiffness gradient in somersault.

A. Modeling *Hydra* body column to represent various steps involved in the somersault movement. **i)** An elastic cylinder comprising of bead-springs is used to model the *Hydra* body column. The cylinder is a stack of 50 rings, each consisting of 10 beads (mass = m). Beads within and from adjacent rings are connected to each other with springs as shown (ii to vi) to maintain circular cross section and resist bending, stretching, torsion and shear. Spring constant of a quarter of the body length (shoulder) is kept α times the rest.

B. For strain ε = 0.8, the plot of the energy in the shoulder region $E_{shoulder}$ versus time (after contraction, see Figure 4 – Figure supplement 2 C) for α = 3 and α = 1. $E_{threshold}$ is the calculated minimum energy required to overcome gravity and viscous drag (see Method detail 4.2). The snapshots show the initial and the final positions of the simulation for α = 1 and α = 3.

C. The plot of time averaged longitudinal force on 14th ring, which is at the junction of the stiff shoulder and rest of the body column with respect to α after the release. The average is taken over 50 ms before and after the end of contraction. This indicates that the optimal energy transfer happens around α = 5. The inset shows force for α =3 and α =1 before the contraction is complete at ~ 50 -100 ms. Initially the force is nearly same in both cases, but it becomes roughly twice for α = 3 at later times. Before the contraction is complete the force is considerably larger for α =3 compared to α=1.

D. The phase diagram to describe the importance of tissue stiffness variation along the body column to overcome downward force on it due to higher density of *Hydra* tissue compared to water. The region represented by crosses is the range of parameters in which model *Hydra* is unable to stand inverted after the release and open circles represents the range in which it is able to stand inverted. The experimentally measured parameters of *Hydra* lie in the green oval in the phase space. The

width and height of the oval represent errors involved in estimating α and *Hydra* density respectively. The strain ε is 0.8.

Figure 5. The stiffness gradient in body column is essential for locomotion through the somersault.

A. The ECM was perturbed locally in *Hydra* polyp using a partial cut (nick) and the stiffness gradient was abolished (represented as + for native state and – for abolished). The time for regeneration after the nick is shown along the arrow and the nick is represented at the appropriate position along *Hydra.* The graph shows the average somersault events per *Hydra* with nicks at the shoulder or the body column (n=20, N=3). Perturbing the stiffness in the shoulder region significantly reduces the somersaults by *Hydra* polyps. The error bars represent standard errors and the significance values are calculated using the 2-tailed paired student's t-test. P-value <0.05 is shown as *, <0.005 is shown as **.

B. The ECM was perturbed globally using chemical disruption of collagens by treatment with 10 mM Dipyridyl (DP). The treatment time in DP is shown along the arrow. The average somersault events per *Hydra* reduce upon treatment with DP for 36 hours and none are observed after treatment with DP for 72 hours. The error bars represent standard errors and the significance values are calculated using the 2-tailed paired student's t-test. P-value <0.05 is shown as *, <0.005 is shown as **.

C. The stiffness was also perturbed by disrupting the ECM with a combination of DP treatment and a partial nick. The organisms were treated with DP for 36 hours as shown along the arrow. The partial nick was done for 24 hours on animals pre-treated with DP for 12 hours as shown in the time line. As shown in the graph, abolishing the stiffness gradient with a combination of physical nick and DP treatment also leads to a reduction in the average number of somersault events observed. The error bars represent standard errors and the significance values are calculated using the 2-tailed paired student's t-test. P-value <0.05 is shown as *, <0.005 is shown as **.

Source Data legends

Figure 2-source data 1: This source data file contains all the Young's modulus data generated by AFM measurement presented in Figure 2 and Figure 2-figure supplement 2.

Figure 3-source data 1: This dataset contains the raw data and the fitted curve data for the change in bending energy in the head region in figure 3. The fit parameters and statistics for the fit are also provided.

Figure 4-source data 1: This source data file contains all the datasets relating to model-*hydra* simulations and *hydra* density calculations presented in Figure 4 and Figure 4 related supplement figures.

Figure 5-source data 1: This source data file contains all the datasets pertaining to quantification of somersaults performed by *hydra* upon partial amputation and Dp treatment from Figure 5 and Figure 5- figure supplement 1. It also contains AFM datasets upon Dp treated and nicked *hydra.*

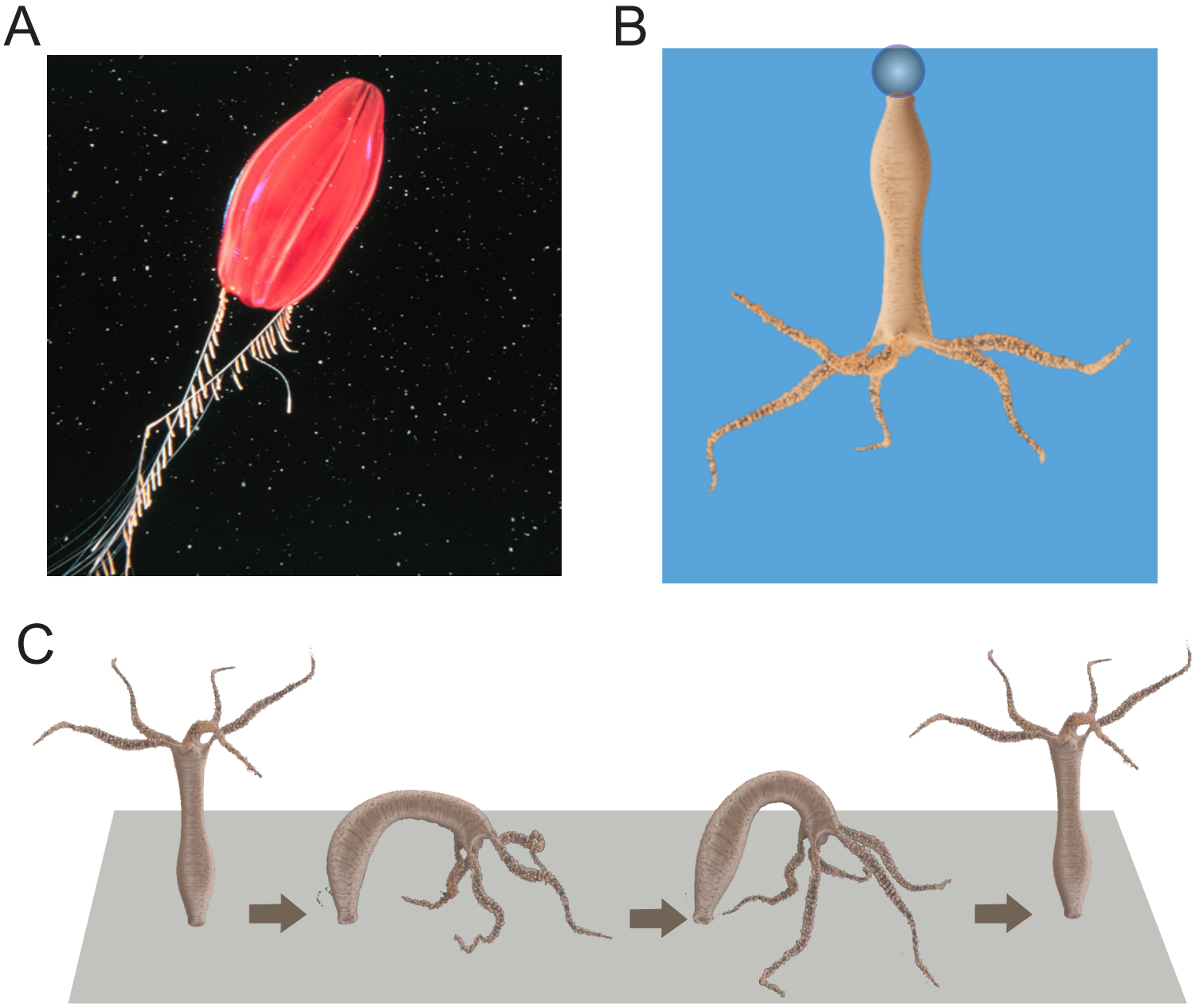

Figure 1. Locomotion in marine invertebrates.

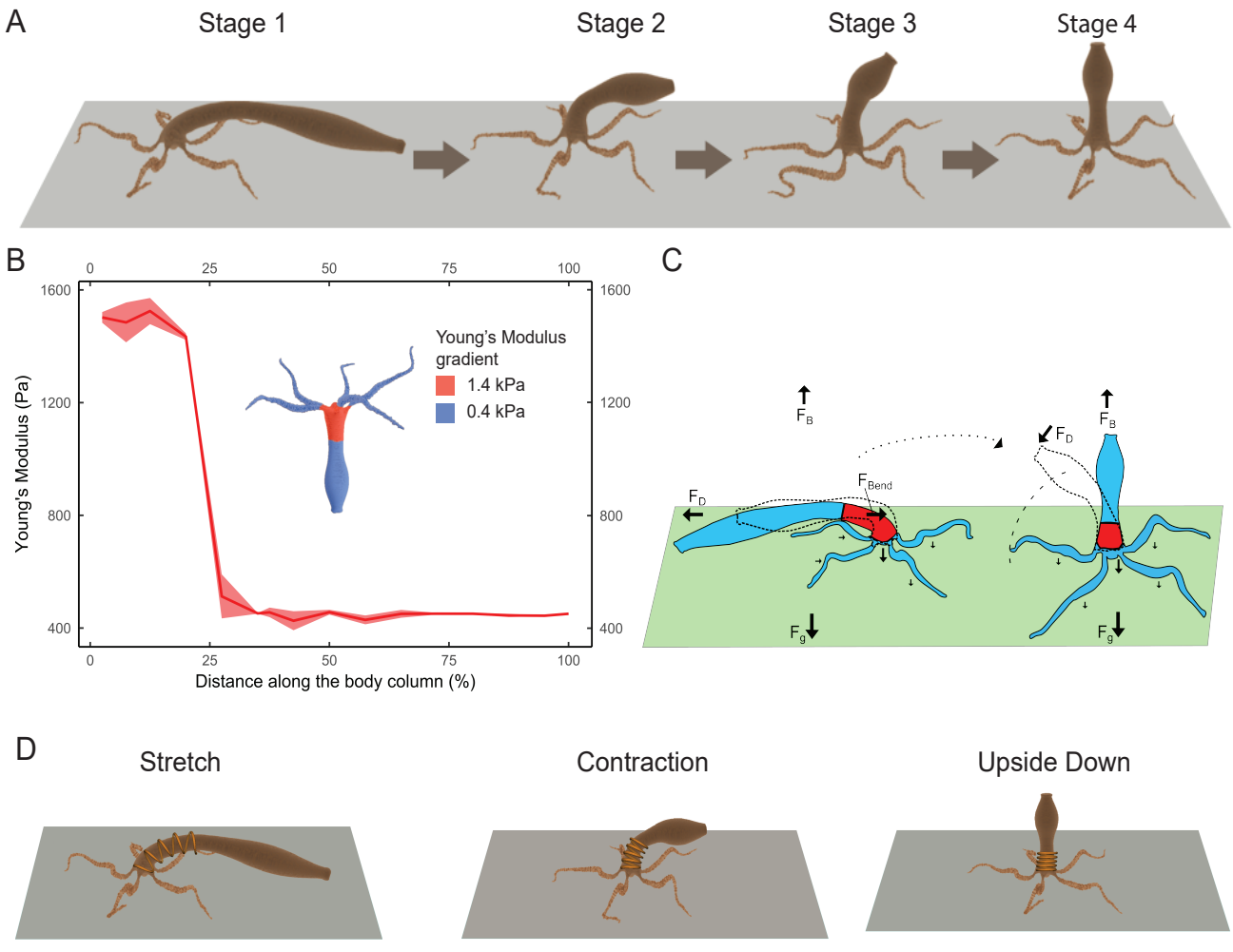

Figure 2. Somersault of Hydra and local variation in tissue stiffness.

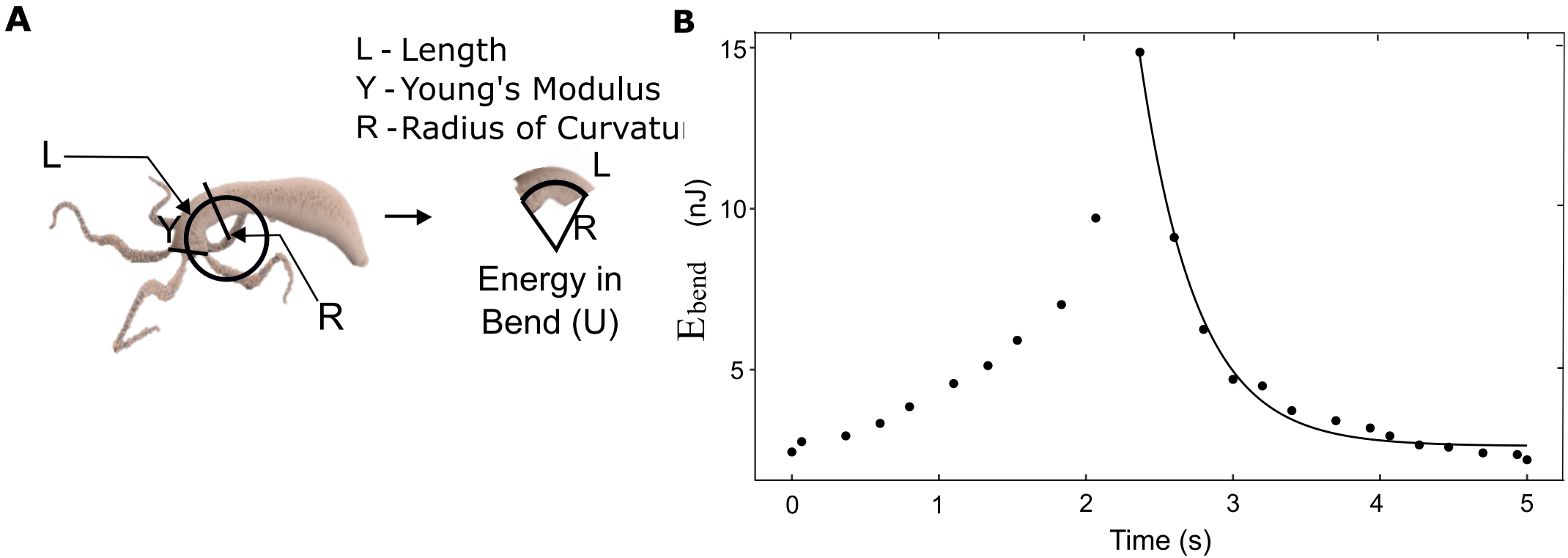

Figure 3. The energy transfer occurring in the stiff shoulder during somersaulting.

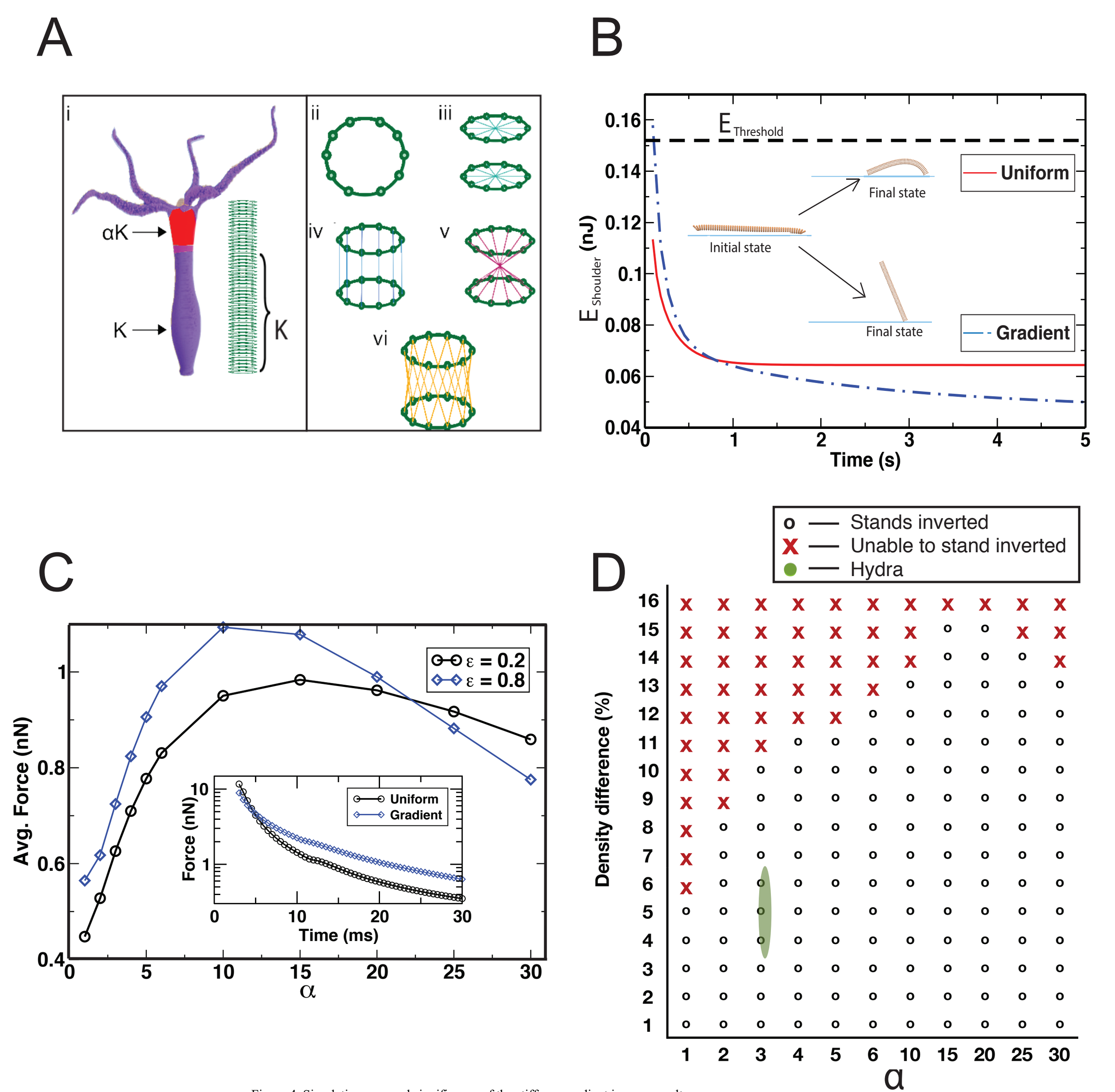

Figure 4. Simulations unravel significance of the stiffness gradient in somersault.

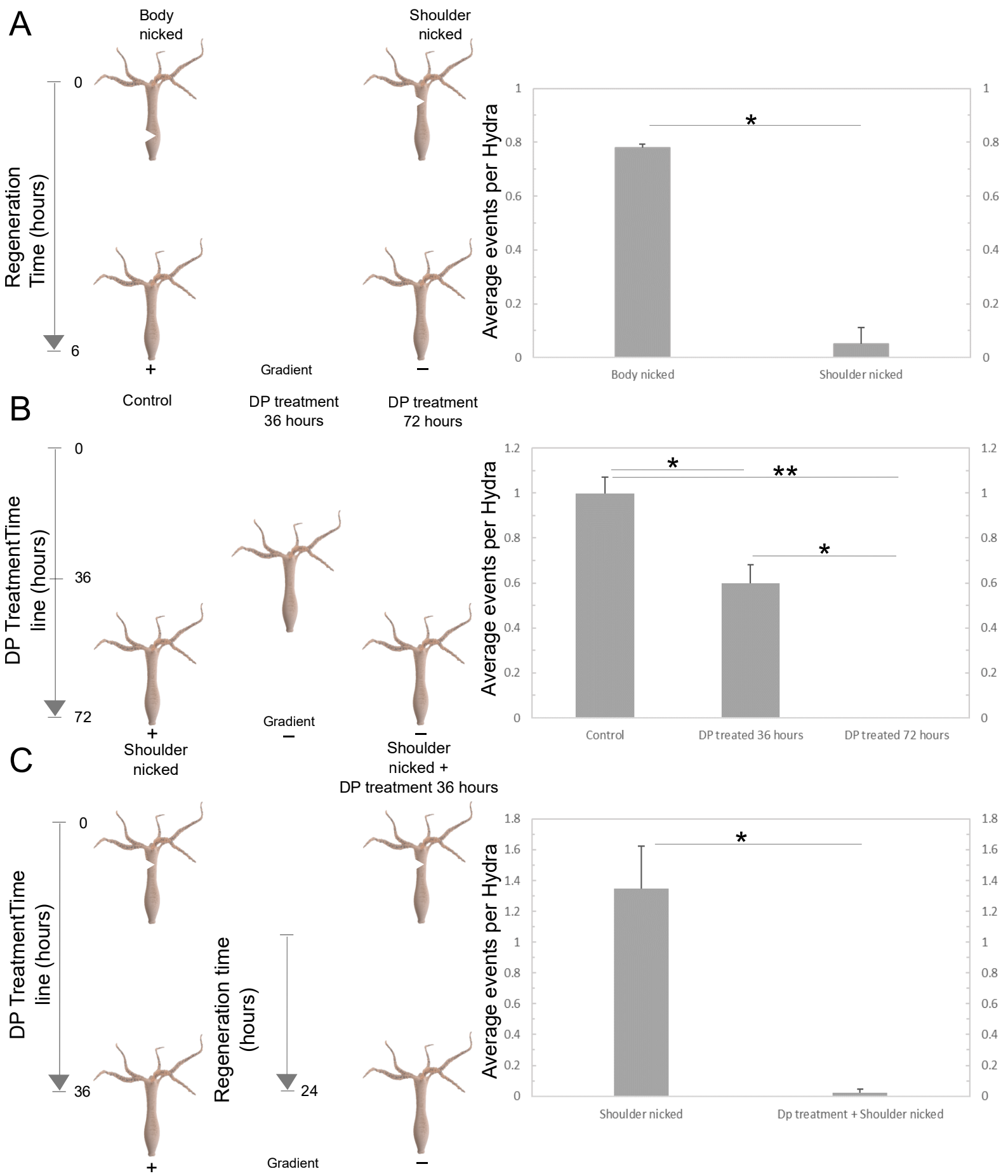

Figure 5. The stiffness gradient in body column is essential for locomotion through the somersault.